Article

Magnetic-composite-modified polycrystalline-silicon nanowire field-effect transistor for vascular endothelial growth factor detection and cancer diagnosis

Hsiao-Chien Chen, Jian-Tai Qiu, Fu-Liang Yang, Yin-Chih Liu, Min-Cheng Chen, Rung-Ywan Tsai, Hung-Wei Yang, Chia-Yi Lin, Chu-Chi Lin, Tzong-Shoon Wu, Yi-Ming Tu, Min-Cong Xiao, Chia-Hua Ho, Chien-Chao Huang, Chao Sung Lai, and Mu-Yi Hua

Anal. Chem., **Just Accepted Manuscript** • DOI: 10.1021/ac5001898 • Publication Date (Web): 19 Mar 2014

Magnetic-composite-modified polycrystalline-silicon nanowire field-effect transistor for vascular endothelial growth factor detection and cancer diagnosis

Hsiao-Chien Chen[†,‡,1], Jian-Tai Qiu[§,1], Fu-Liang Yang[∥,1], Yin-Chih Liu[†], Min-Cheng Chen[∥], Rung-Ywan Tsai[⊥], Hung-Wei Yang[†], Chia-Yi Lin[∥], Chu-Chi Lin[§], Tzong-Shoon Wu[§], Yi-Ming Tu[†], Min-Cong Xiao[†], Chia-Hua Ho[∥], Chien-Chao Huang[∥], Chao-Sung Lai*[,#], and Mu-Yi Hua*[,†]

[†] Department of Chemical and Materials Engineering, Chang Gung University;

Biosensor Group, Biomedical Engineering Research Center, Chang Gung University, Taoyuan, 33302, Taiwan R.O.C.

[‡] Department of Biochemistry, School of Medicine, Taipei Medical University, Taipei, 11031, Taiwan R.O.C.

[§] Department of Biomedical Sciences, School of Medicine, Chang Gung University;

Department of Obstetrics and Gynecology, Chang Gung Memorial Hospital. Taoyuan 33302, Taiwan, R.O.C.

[‖]National Nano Device Laboratories, Hsinchu Science Park, Taiwan, R.O.C.

[⊥] Electronics and Optoelectronics Research Laboratories, Industrial Technology Research Institute, Hsinchu 31040, Taiwan R.O.C.

[#] Department of Electronic Engineering, Chang Gung University

Biosensor Group, Biomedical Engineering Research Center, Chang Gung University. Taoyuan, 33302, Taiwan R.O.C.

[*] Author to whom correspondence should be addressed. Mu-Yi Hua, Phone: +886-3-2118800, ext. 5289; Fax: +886-3-2118668; E-mail: huamy@mail.cgu.edu.tw. Chao-Sung Lai, Phone: +886-3-2118800, ext. 5786; Fax: +886-3-2118507; E-mail: cslai@mail.cgu.edu.tw.

[1] H.-C. C., J.-T. Q., and F.-L. Y. contributed equally to this work.

ABSTRACT: This study proposes a vascular endothelial growth factor (VEGF) biosensor for diagnosing various stages of cervical carcinoma. In addition, the VEGF concentrations at various stages of cancer therapy are determined and compared to data obtained using computed tomography (CT) and cancer antigen 125 (CA-125). The increase in VEGF concentrations during operations offers useful insight into dosage timing during cancer therapy. This biosensor uses Avastin as the biorecognition element for the potential cancer biomarker VEGF and is based on a *n*-type polycrystalline silicon nanowire field-effect transistor (poly-SiNW-FET). Magnetic nanoparticles with poly[aniline-co-*N*-(1-one-butyric acid) aniline]-Fe_3O_4 (SPAnH-Fe_3O_4) shell-core structures are used as carriers for the Avastin loading and provide rapid purification due to their magnetic properties, which prevent the loss of bioactivity; furthermore, the high

surface area of these structures increases the quantity of Avastin immobilized. The average concentrations in human blood for species that interfere with the detection specificity are also evaluated. The detection range of the biosensor for serum samples covers the results expected from both healthy individuals and cancer patients.

KEYWORDS. magnetic nanoparticles; VEGF; poly-SiNW-FET; biosensor; Avastin; cancer

1. INTRODUCTION

Angiogenesis is the process of forming a mature cardiovascular system through a series of complex changes to an embryonic vascular system, including the differentiation, migration, and association of primitive endothelial cells.[1,2] This activity is necessary in adults to repair normal tissues and to remodel female reproductive organs. In addition, this process is highly controlled by angiogenic balances, such as the physiological balance between stimulatory and inhibitory signals for blood vessel growth.[3] However, under pathological conditions, uncontrolled angiogenesis results from cancer, diabetes, arthritis, ocular neovascularization, and several other diseases due to local changes in the balance between angiogenic stimulators and inhibitors.[4–7]

Various tumor cells secrete excess proangiogenic growth factors for tumor vascularization. Of the known angiogenic factors, vascular endothelial growth factor (VEGF) is active for angiogenesis, vasculogenesis, and endothelial cell growth and thus increases the proliferation of endothelial cells, promotes cell migration, inhibits apoptosis, and induces blood vessel permeabilization.[8] VEGF has been associated with the progression and poor prognosis of several tumors, including cervical cancer.[9] Cervical cancer cells exhibit higher VEGF intratumoral protein levels than normal cervical tissues. In addition, this higher VEGF level increases the risk of lymph node metastasis. Thus, malignant tumors are often diagnosed using the VEGF protein levels in blood.

With these considerations in mind, several systems for detecting VEGF have been developed based on enzyme-linked immunosorbent assay (ELISA),[10] fluorescence,[11] electrochemical technologies,[12] surface plasmon resonance,[13] surface-enhanced Raman scattering,[14] and field-effect transistor (FET) techniques.[15,16] Nanowire-based FETs are one of the most promising platforms among these systems for label-free sensing due to their potential

advantages for miniaturization, high specificity, and superior sensitivity when detecting charged biomolecules. Hence, FETs are being increasingly used to develop biosensors to identify metal ions, nucleic acids, penicillin, and viruses.[17–20] The immobilization of artificial biological components on silicon nanowire (SiNW)-FET surfaces yields a high affinity, specificity, and selectivity for specific target molecules.

Avastin (bevacizumab) is a humanized monoclonal antibody of VEGF.[2,3] As an agent approved by the U.S. Food and Drug Administration (FDA), Avastin is widely used in the targeted therapy of metastatic colorectal cancer,[21] advanced ovarian cancer,[22] renal cell carcinoma,[23] and non-small-cell lung cancer.[24] The principal action of Avastin is to inhibit the natural protein VEGF, which stimulates new blood vessel formation, and it is recognized as an extremely potent angiogenesis inhibitor. Due to its specificity for VEGF, the current study used Avastin immobilized on a shell-core nanoparticle, poly[aniline-co-*N*-(1-one-butyric acid) aniline]-Fe_3O_4 (SPAnH-Fe_3O_4), to develop a modified *n*-type polycrystalline SiNW-FET (poly-SiNW-FET). SPAnH-Fe_3O_4 nanoparticles are considered to be nontoxic to human umbilical vein endothelial cells (HUVECs).[25] These biocompatible nanoparticles have been widely researched as nanocarriers for the targeted delivery of drugs during cancer therapy.[26,27] Nanocarriers provide a high surface area for drug loading, and the immobilized drugs are more thermally stable than free drugs. In addition, the bound drug is rapidly separated and purified by an applied magnetic field, which reduces the risk of denaturation.[28] The presence of SPAnH can prevent the aggregation of nanoparticles and maintain their stability in aqueous solutions. Here, SPAnH-Fe_3O_4-nanoparticle-modified poly-SiNW-FETs were developed to determine VEGF due to their abundant bioactive sites and their carboxylic groups, which allow the SPAnH-Fe_3O_4 nanoparticles to covalently bind Avastin. Finally, the practical application of the proposed

biosensor was evaluated by determining the VEGF levels in human serum samples, including both healthy people and patients with cervical or ovarian carcinoma.

2. EXPERIMENTAL SECTION

2.1. Modification of poly-SiNW-FET and fabrication of biochip. The functional modification of the poly-SiNW-FET with terminal amine groups was performed as follows. A 5 μL solution of 2 wt% APTES in ethanol was placed on the poly-SiNW for 1 h to form a self-assembled monolayer. The modified chip was then washed with ethanol and dried in an oven at 100 °C for 1 h. To add the Avastin-SPAnH-Fe_3O_4, the chip was further treated with 5% glutaraldehyde at room temperature for 1 h, which formed the terminal aldehyde groups for direct Avastin-SPAnH-Fe_3O_4 immobilization after adding the magnetic nanoparticles to the poly-SiNW-FET for 1 h. To eliminate non-specific adsorption and residual aldehyde groups, 5 μL of bovine serum albumin (BSA, at a 5 mg/mL concentration in PBS as a blocking buffer) was added to the biochip at 4 °C for 1 h in dark environment. After a final wash with PBS for three times, samples were assayed as described.

2.2. VEGF detection on Avastin-SPAnH-Fe_3O_4/poly-SiNW-FET. We used the response current of the FET in 0.5 mM PBS as the baseline current. The h-$VEGF_{165}$ standard was injected into the microfluid channel and reacted for 10 min in the dark at room temperature. The unreacted h-$VEGF_{165}$ was removed by washing for three times, and PBS was re-injected into the microfluid channel prior to the measurement. The detection of VEGF in the sera of patients with ovarian cancer was performed using three distinct consecutive steps, i.e., reaction, washing, and quantification. Initially, samples were washed three times with PBS according to the standard

procedure. In all cases, the sample drop volume applied onto the biochip was 5 μL. All of the measurements were obtained using a 50 mV bias voltage, V_B. We chose a current at a constant gate voltage (V_G = 2.4 V) as the criterion to quantify the h-$VEGF_{165}$.

3. RESULTS AND DISCUSSION

3.1. Immobilization and characterization of Avastin-SPAnH-Fe_3O_4. Figure 1a presents a scheme of the prepared SPAnH-Fe_3O_4 nanoparticles and immobilized Avastin. The average size of the prepared Fe_3O_4 particles was approximately 10 nm (Figure 1b); this size did not increase noticeably after coating SPAnH onto the surface (Figure 1c). The presence of SPAnH was confirmed via Fourier transform infrared (FT-IR) spectroscopy (Figure 1d). The characteristic peak for Fe_3O_4 was observed at 588 cm^{-1} and is attributed to the stretching mode of Fe–O. The additional peaks at 1,593, 1,310, and 1,157 cm^{-1} were assigned to the stretching vibrations of C=C, C–N, and N=Q=N from SPAnH, respectively, which indicates that SPAnH-Fe_3O_4 was successfully prepared. The quantity of carboxylic groups (–COOH) on the nanoparticle surface, measured using toluidine blue-O (TBO), was approximately 3.1 μmol per mg of SPAnH-Fe_3O_4. This high carboxyl concentration favors the immobilization of biomolecular compounds. For VEGF, Avastin was chosen as the biorecognition element and covalently immobilized on the SPAnH-Fe_3O_4 through an EDC/sulfo-NHS linkage (Figure 1a). The absorption bands of the functional groups were used to probe the secondary structure of the polypeptide chain to determine the bioactivity of the immobilized Avastin. The immobilized Avastin peaks in the functional and fingerprint regions were similar to those of free Avastin, indicating that the conformation was maintained during immobilization. This result can be attributed to the rapid purification process. The free biomolecules are traditionally separated from those immobilized on

carriers *via* high-speed centrifugation. However, the generated heat is detrimental to the bioactivity. In contrast, the simple, rapid separation of Avastin-SPAnH-Fe_3O_4 was achieved by applying a magnetic field, which avoids the risk of denaturation and preserves the native bioactivity.

The interfacial effect of Avastin-SPAnH-Fe_3O_4 on a gold electrode was also investigated via electrochemical impedance spectroscopy (EIS) in 1 mM $Fe(CN)_6^{3-/4-}$ (Figure 1e). The data from the bare electrode were approximately linear, which is characteristic of a diffusion-limited electrochemical process.[29] The charge transfer resistance increased to 60 kΩ after modification with SPAnH-Fe_3O_4, indicating the electrostatic repulsion of the negative redox probe $Fe(CN)_6^{3-/4-}$ by a negative dissociated carboxylic group, $–COO^–$. The resistance increased further to 80 kΩ upon Avastin-SPAnH-Fe_3O_4 binding, indicating that the Avastin surrounded the SPAnH-Fe_3O_4 surface and possessed more negative charges.

In addition, the optimal loading on 50 μg of SPAnH-Fe_3O_4 was determined by reactions with various Avastin concentrations. The Avastin loading can be calculated via an ELISA of the free Avastin using a monitoring wavelength of 450 nm. As shown in Figure 1f, the loading clearly increased with increasing Avastin concentrations of up to 500 μg/mL of MES buffer, where saturation occurred. These results indicate that 18 μg of Avastin can be loaded onto 50 μg of SPAnH-Fe_3O_4.

3.2. Preparation and characterization of poly-SiNW-FET. The poly-SiNW-FET biosensors were based on the principle of sensing through variations in the conductance caused by surface charge disturbances. Various wire lengths and widths were developed via the CMOS process described in the experimental section to optimize the sensing performance. Figure 2a presents an image of the fabricated poly-SiNW-FET. The six-inch wafer can be segmented into 32 chips,

with 18 devices on each chip. Figure 2b presents a schematic diagram of the poly-SiNW-FET device. The wire lengths and widths for each device were 0.4~13 μm and 0.3~0.5 μm, respectively. For example, Figure 2c presents a poly-SiNW-FET device with a 2 μm long, 0.3 μm wide wire. These devices were tested in 0.5 mM PBS because most biological interactions occur under aqueous conditions, and the transfer characteristics of the devices were analyzed using V_G values of 1.5~2.0 V (Figure 2d). The 2 μm long, 0.3 μm wide wire yielded a maximum conductance of 1.27 μS, indicating its high sensitivity.

The surface of the highly sensitive device was further modified using (3-aminopropyl)triethoxysilane (APTES) and glutaraldehyde (GA) to provide terminal aldehyde groups for immobilizing the Avastin-SPAnH-Fe_3O_4 probe (Figure 3a). In this case, the devices were passivated by BSA to prevent non-specific reactions or binding (Figure 3b). The device sensitivity was further confirmed by loading Avastin-SPAnH-Fe_3O_4 onto a poly-SiNW-FET and hybridizing with 125 pg/mL VEGF for 10 min. The efficient detection range of a FET biosensor is known to be located within the Debye length, which is relative to the ionic strength of the solution. Higher ion concentrations yield shorter Debye lengths and shield the charged surface. To match the size of the Avastin-SPAnH-Fe_3O_4 nanoparticle, 0.5 mM PBS with a Debye length of approximately 15.2 nm was used for charge screening. The current of the device with the highest conductance decreased from 1.16 μA to 0.74 μA, corresponding to a 36.2% decrease in the relative current ($-\Delta I/I_0$ %), the highest among all of the devices (Figure 3c). This phenomenon of decreasing conductance and thus increasing resistance accounts for the few positive charge carriers present in the *n*-type poly-SiNW-FET. When negatively charged VEGF binds to the probe, it attracts carriers from the substrate to the channel, which decreases the conductance between the source and drain electrodes.[30] In addition, the sensitivity to VEGF is directly

correlated to the device conductance, i.e., a higher conductance corresponds to a higher sensitivity.[31]

3.3. Performance of Avastin-SPAnH-Fe_3O_4/poly-SiNW-FET biosensors for the detection of VEGF. Real-time FET biosensors have been previously developed based on changes in the current measured after injecting specific analytes.[32–35] The receptors on the surface of such devices are exposed to solutions containing charged biomolecules, such as proteins or viruses, for specific binding that increases or decreases the conductance. However, without further purification, the real-time change in conductance is affected by both binding and non-binding species, particularly for analytes from samples containing unpredictably charged biomolecules within the Debye length. In this study, additional washing and alternation with PBS was performed after hybridization prior to measurement to eliminate the influence of free VEGF and other interfering species in the serum. The changes in the current depended on the VEGF binding and accurately related the I_{SD} and VEGF levels. The current clearly changed in the presence of interfering species, such as immunoglobulin G (IgG, 1,000 ng/dL), immunoglobulin M (IgM, 192.5 mg/dL), glucose (5 mM), ascorbic acid (AA, 4.3 μg/mL), and uric acid (UA, 0.295 mM) (Figures 4a and 4b). The concentrations of these interfering species are typical of human plasma.[36–39] Although these species continued to induce a small current response after washing, perhaps due to a small amount of nonspecific adsorption, the washes significantly reduced their influence on the measurements. Using an injection–hybridization–wash–measurement procedure, the current decreased with increasing VEGF concentrations due to the depletion of charge carriers in the poly-SiNW-FET when the negatively charged VEGF (ζ-potential, –5.7 mV) was bound to the Avastin-functionalized surface (Figure 4c). Figure 4d presents the change in current

as a function of the VEGF concentration. The lowest VEGF concentration detected (an 11.5% current decrease) and differentiated from the noise level (a 10% current decrease) based on the maximal influence of 1,000 ng/dL IgG was approximately 1.25 pg/mL. The current increased linearly upon increasing the VEGF concentration from 6.25 pg/mL to 500 ng/mL, indicating that the response was the direct result of VEGF binding to Avastin. Furthermore, various VEGF concentrations in the above interfering species were evaluated. Although these values affect the presence of interfering species, these variations were insignificant. The binding constant of the hybridization between Avastin and VEGF was investigated using the Langmuir adsorption isotherms, which are widely used to estimate the binding affinity of antigen-antibody interactions.[40] Accordingly, the reaction between Avastin and VEGF on a poly-SiNW-FET followed the Langmuir adsorption isotherm given by

$$\Delta I_{SD} = \frac{\Delta I_{SD,\max} C_{VEGF}}{K_D + C_{VEGF}} \quad (1)$$

where $\Delta I_{SD,max}$ and C_{VEGF} are the saturated net changes in the drain-source current and VEGF concentration, respectively, and K_D is the binding constant for the Avastin and VEGF protein interactions. The binding constant for VEGF to the Avastin-SPAnH-Fe_3O_4/poly-SiNW-FET biosensor was estimated to be 4.48 ng/mL assuming negligible intermolecular interactions between the immobilized Avastin and uniform binding sites (i.e., equal binding energy) on the nanoparticle surface. This experiment was the first successful determination of the VEGF-Avastin binding energy.

In previous reports, Avastin was directly immobilized onto the nanowire for hybridization with VEGF. However, biomacromolecules obviously had steric hindrance under such a confined one-dimensional environment, ultimately decreasing the degree of immobilization and

hybridization. The SPAnH-Fe_3O_4 nanoparticles used in our study contain numerous active sites (e.g., carboxylic groups) that are able to immobilize Avastin. The freely suspended SPAnH-Fe_3O_4 nanoparticles successfully increased the degree of immobilization. In addition, the rapid separation caused by the application of an additional magnetic field was able to preserve the original bioactivity. In the detection of VEGF, the curvature of the nanoparticle surfaces formes a three-dimensional structure that provides a high surface area and decreases steric hindrance, ultimately increasing the degree of immobilization and hybridization. The aforementioned features (including high bioaffinity and surface areas) improves Avastin bioactivity, ultimately making the proposed VEGF biosensor superior to previous similar devices in terms of specificity across a wide detection range.[12,15,16,41]

3.4. Reproducibility and stability of the VEGF biosensor. The reproducibility of the biosensor was tested by repeating the experimental procedures in triplicate, including the Avastin immobilization, poly-SiNW-FET modification, and VEGF determination (125 pg/mL). The relative responses indicate an acceptable relative standard deviation of 6.4%. The Avastin-SPAnH-Fe_3O_4/poly-SiNW-FET stability at 4 °C in a dry state was also investigated for various storage times prior to the VEGF measurements (125 pg/mL). Excluding the relative standard of deviation from the reproducibility tests, the biosensor retained 76.4% of its initial relative current response after 10 days (Figure 5). The free protein suffered from denaturation and conformational changes caused by the surrounding conditions, such as the buffer solution and temperature.[42] The immobilization of Avastin on SPAnH-Fe_3O_4 may limit its ability to undergo drastic conformational changes and thus increase its resistance toward denaturation. Thus, the

stability of Avastin can be attributed to its firm immobilization on SPAnH-Fe_3O_4 and the biocompatible microenvironment.

3.5. Determination of VEGF in human serum. VEGF is critical for cancer growth and metastasis and is often overexpressed in tumors.[43–45] Therefore, patients with various solid tumors typically have higher serum concentrations of soluble VEGF than healthy individuals.[43,46,47] Cervical carcinoma is a common gynecologic malignancy worldwide. Serum samples were collected from patients diagnosed with different stages of noninvasive cervical carcinoma (n = 18) to assess the utility of the VEGF biosensor based on an Avastin-SPAnH-Fe_3O_4/poly-SiNW-FET for clinical analyses. The assessment results are presented in Figure 6a. The average VEGF concentrations for stages I, II, and III-IV were approximately 262, 537, and 851 pg/mL, respectively. The values detected using the proposed biosensors were comparable to those obtained from classical ELISA. These results indicate that the developed biosensor is reliable with high selectivity and demonstrate the relationship between the VEGF concentration and cancer stage, with increasing concentrations with the progression of cancer from stage I to IV.[12,41] Furthermore, individual samples from healthy subjects were analyzed (Figure 6b), and the proposed biosensor indicated that the VEGF concentrations were all approximately 100 pg/mL. Unfortunately, these relatively low concentrations could not be assayed using ELISA (Figure 6c). Therefore, the proposed VEGF biosensor using an Avastin-SPAnH-Fe_3O_4/poly-SiNW-FET is preferred when comparing VEGF variations in healthy subjects to those of cancer patients.

3.6. Monitoring the VEGF of a patient suffering from ovarian cancer. Ovarian carcinoma is one of the most common gynecologic malignancies and causes over half of all cancer-related deaths, making it the most lethal of such tumors.[48] The high mortality rate of this cancer indicates

the importance of early diagnosis. The role of VEGF in ovarian carcinoma has been established by many researchers reporting high VEGF levels in the plasma and ascites of patients.[49] VEGF is overexpressed in a variety of tumors, which causes malignant ascites in the peritoneal cavity that facilitate the multifocal dissemination of the ovarian tumor cells to the intraperitoneal surface and may directly influence the clinical course.[50] The VEGF concentrations in sera from a single patient with ovarian carcinoma at various stages, including pre-operation, post-operation, and after Avastin therapy, were traced using the proposed biosensor and compared to the computed tomography (CT) and cancer antigen 125 (CA-125) analysis results (Figure 7 and inset). In the pre-operative region (yellow), the CT results indicate that the tumor size in the pelvis was approximately 10.6 cm with a high VEGF concentration (2,290 pg/mL) and CA-125 response (8,921 U/mL). The CA-125 value suddenly decreased after the operation (green region). The CA-125 and CT values slowly decreased further after Avastin therapy (white region). The VEGF concentrations approximately corresponded to the data determined using CT and CA-125, indicating that the developed biosensor is capable of monitoring VEGF concentrations in various states. Interestingly, an abnormally high post-operation VEGF concentration was observed relative to the pre-operation condition, whereas the CT and CA-125 values decreased. This result indicates that the VEGF concentration increases during operation and illustrates an important concern regarding the probability of tumor relapse after an operation, which could lead to additional clinical research on dosage timing.

4. CONCLUSIONS

In summary, a label-free electrical method for detecting VEGF was developed using a prepared Avastin-SPAnH-Fe_3O_4/poly-SiNW-FET biosensor. SPAnH-Fe_3O_4 magnetic

nanoparticles with shell-core structures provide a high surface area for Avastin loading and have rapid purification, which prevents denaturation. Although the specific target is commonly used, an additional wash to remove any un-hybridized VEGF or other interfering species ensures the sensor's accuracy and improves its detection for individual samples. The Avastin-SPAnH-Fe_3O_4/poly-SiNW-FET biosensor was also used to diagnose patients suffering from cervical cancer at stages I to III-IV, demonstrating the correlation between the VEGF concentration and the stage of cervical cancer. These results are promising, comparable to those obtained using the ELISA method and confirm that the developed biosensor has the potential to provide a useful analytical approach for cancer diagnoses. Finally, tracking the VEGF concentrations in a patient with ovarian carcinoma across various therapeutic stages demonstrates the potential for additional applications and offers a useful basis for the timing of cancer therapies.

ASSOCIATED CONTENT

Supporting Information

Experimental materials and protocols are available free of charge *via* the Internet at http://pubs.acs.org.

ACKNOWLEDGEMENT

We thank the National Science Council of the Republic of China, Chang Gung University, and the Industrial Technology Research Institute for their financial support: NSC 101-2221-E-182-011-MY3, CMRPD2D0081, NSC 100-2221-E-182-005, CMRPD2A0062,

UERPD2B0281, and AF51RQ3000. We also thank Chang Gung Memorial Hospital Microscopy Core Laboratory.

REFERENCES

(1) Coultas, L.; Chawengsaksophak, K.; Rossant, J. *Nature* **2005,** 438, 937–945.

(2) Yancopoulos, G. D. *Cell* **2010**, *143*, 13–16.

(3) Bagri, A.; Kouros-Mehr, H.; Leong, K. G.; Plowman, G. D. *Trends Mol. Med.* **2010**, *16*, 122–132.

(4) Koch, A. E. *Arthritis Rheum*. **1998**, *41*, 951–962.

(5) Folkman, J. *J. Nat. Cancer Inst.* **1990**, *82*, 4–6.

(6) Carmellet, P.; Jain, R. K. *Nature* **2000**,*407*, 249–257.

(7) Fitzgerald, K. T.; Holladay, C. A.; McCarthy, C.; Power, K. A.; Pandit, A.; Gallagher, W. M. *Small* **2011**, *7*, 705–717.

(8) Roskoski, R. J. *Crit. Rev. Oncol. Hemat.* **2007**, *62,* 179–213.

(9) Shi, K.; Xi, L.; Weng, D.; Chen, G.; Song, X.; Wu, P.; Wang, B.; Wei, J.; Wang, S.; Zhou, J.; Ma, D. *Int. J. Biomed. Sci.* **2008**, *4*, 58–63.

(10) Pavlakovic, H.; Von Schütz, V.; Rössler, J.; Koscielniak, E.; Havers, W.; Schweigerer, L. *Int. J. Cancer.* **2001**, *92*, 756–760.

(11) Cho, H.; Yeh, E. C.; Sinha, R.; Laurence, T. A.; Bearinger, J. P.; Lee, L. P. *ACS Nano*, **2012**, 6, 7607–7614.

(12) Zhao, S.; Yang, W.; Lai, R. Y. *Biosens. Bioelectron*. **2011**, *26*, 2442–2447.

(13) Li, Y.; Hye, J. L.; Corn, R. M. *Anal. Chem.* **2007**, *79*, 1082–1088.

(14) Li, M.; Cushing, S. K.; Zhang, J.; Suri, S.; Evans, R.; Petros, W. P.; Gibson, L. F. Ma, D.; Liu, Y.; Wu, N. Q. *ACS Nano*, **2013**, 7, 4967–4976.

(15) Kwon, O. S.; Park, S. J.; Hong, J. T.; Han, A. R.; Lee, J. S.; Lee, J. S.; Oh, J. H.; Jang, J. *ACS Nano*, **2012**, 6, 1486–1493.

(16) Lee, H. S.; Kim, K. S.; Kim, C. J.; Hahn S. K.; Jo, M. H. *Biosens. Bioelectron.* **2009**, *24*, 1801–1805.

(17) Makowski, M. S.; Ivanisevic, A. *Small* **2011**, *7*, 1863–1875.

(18) Gao, A.; Lu, N.; Dai, P.; Li, T.; Pei, H.; Gao, X.; Gong, Y.; Wang, Y.; Fan, C. *Nano Lett*. **2011**, *11*, 3974–3978.

(19) Buth, F.; Donner, A.; Sachsenhauser, M.; Stutzmann, M.; Garrido, J. A. *Adv. Mater.* **2012,** 24, 4511–4517.

(20) Stern, E.; Klemic, J. F.; Routenberg, D. A.; Wyrembak, P. N.; Turner-Evans, D. B.; Hamilton, A. D.; LaVan, D. A.; Fahmy, T. M.; Reed, M. A. *Nature* **2007**, *445*, 519–522.

(21) Rugo, H. S. *Oncologist* **2004**, *9*, 43–49.

(22) Yap, T. A.; Carden, C. P.; Kaye, S. B. Nat. Rev. *Cancer* **2009**, *9*, 167–181.

(23) Summers, J.; Cohen, M. H.; Keegan, P.; Pazdur, R. *Oncologist* **2010**, *15*, 104–111.

(24) Sandler, A.; Gray, R.; Perry, M. C.; Brahmer, J.; Schiller, J. H.; Dowlati, A.; Lilenbaum, R.; Johnson, D. H. *N. Eng. J. Med.* **2006**, *355*, 2542–2550.

(25) Hua, M. Y.; Liu, H. L.; Yang, H. W.; Chen, P. Y.; Tsai, R. Y.; Huang, C. Y.; Tseng, I. C.; Lyu, L. A.; Ma, C. C.; Tang, H. J.; Yen, T. C.; Wei, K. C. *Biomaterials* **2011**, *32*, 516–527.

(26) Yang, H. W.; Hua, M. Y.; Liu, H. L.; Tsai, R. Y.; Pang, S. T.; Hsu, P. H.; Tang, H. J.; Yen, T. C.; Chuang, C. K. *Biomaterials* **2012**, *33*, 3919–3930.

(27) Yang, H. W.; Hua, M. Y.; Liu, H. L.; Tsai, R. Y.; Chuang, C. K.; Chu, P. C.; Wu, P. Y.; Chang, Y. H.; Chuang, H. C.; Yu, K. J.; Pang, S. T. *ACS Nano* **2012**, *6*, 1795–1805.

(28) Pérez-López, B.; Merkoçi, A. *Adv. Funct. Mater.* **2011**, 21, 255–260.

(29) Ivnitski, D.; Wilkins, E.; Tien, H. T.; Ottova, A. *Electrochem. Commun.* **2000**, *2*, 457–460.

(30) Zhang, G. J.; Zhang, G.; Chua, J. H.; Chee, R. E.; Wong, E. H.; Agarwal, A.; Buddharaju, K. D.; Singh, N.; Gao, Z.; Balasubramanian, N. *Nano Lett.* **2008**, *8*, 1066–1070.

(31) Kwon, O. S.; Park, S. J.; Jang, J. *Biomaterials* **2010,** 31, 4740–4747.

(32) He, Q.; Wu, S.; Gao, S.; Cao, X.; Yin, Z.; Li, H.; Chen, P.; Zhang, H. *ACS Nano* **2007**, *5*, 5038–5044.

(33) Huang, S. C.; Artyukhin, A.; Misra, M.; Martinez, J.; Stroeve, P.; Grigoropoulos, C.; Ju, J.; Noy, A. *Nano Lett*. **2010**, *10*, 1812–1816.

(34) Oh, J.; Chang, Y. W.; Kim, H. J.; Yoo, S.; Kim, D. J.; Im, S.; Park, Y. J.; Kim, D.; Yoo, K. H. *Nano Lett*. **2010**, *10*, 2755–2760.

(35) Chen, C. C.; Chen, Y. Z.; Huang, Y. J.; Sheu, J. T. *Biosens. Bioelectron.* **2011**, *26*, 2323–2328.

(36) Murphy, K.; Travers, P.; Walport, M. *Janeway's Immino biology*, Garland Science, New York and London 2008.

(37) Marquette, C. A.; Degiuli, A.; Blum, L. J. *Biosens. Bioelectron.* **2003**, *19*, 433–439.

(38) Khan, A.; Khan, M. I.; Iqbal, Z.; Shah, Y.; Ahmad, L.; Nazir, S.; Watson, D. G.; Khan, J. A.; Nasir, F.; Khan, A. *Talanta* **2011**, *84*, 789–801.

(39) Raj, C. R.; Ohsaka, T. *J. Electroanal. Chem.* **2003**, *540*, 69–77.

(40) Abe, M.; Murata, K.; Kojima, A.; Ifuku, Y.; Shimizu, M.; Ataka, T.; Matsumoto, K. *J. Phys. Chem. C* **2007**, *111*, 8667–8670.

(41) Prabhulkar, S.; Alwarappan, S.; Liu, G.; Li, C. Z. *Biosens. Bioelectron.* **2009**, *24*, 3524–3530.

(42) Hong, J.; Xu, D.; Gong, P.; Yu, J.; Ma, H.; Yao, S. *Micropor. Mesopors Mat.* **2008**, *109*, 470–477.

(43) Barton, D. P. J.; Cai, A.; Wendt, K.; Young, M.; Gamero, A.; De Cesare, S. *Clin. Cancer Res.* **1997**, *3*, 1579–1586.

(44) Kassim, S. K.; El-Salahy, E. M.; Fayed, S. T.; Helal, S. A.; Helal, T.; Azzam, E. D.; Khalifa,

A. *Clin. Biochem.* **2004**, *37*, 363–369.

(45) Kido, S.; Kitadai, Y.; Hattori, N.; Haruma, K.; Kido, T.; Ohta, M.; Tanaka, S.; Yoshihara, M.; Sumii, K.; Ohmoto, Y.; Chayama, K. *Eur. J. Cancer* **2001**, *37*, 1482–1487.

(46) Matsuyama, W.; Hashiguchi, T.; Mizoguchi, A.; Iwami, F.; Kawabata, M.; Arimura, K.; Osame, M. *Chest* **2000**, *118*, 948–951.

(47) Liu, C. D.; Tilch, L.; Kwan, D.; McFadden, D. W. *J. Surg. Res.* **2002**, *102*, 31–34.

(48) Feki, A.; Berardi, P.; Bellingan, G.; Major, A.; Krause, K. H.; Petignat, P.; Zehra, R.; Pervaiz, S.; Irminger-Finger, I. *Crit. Rev. Oncol. Hematol.* **2009**, *72*, 1–9.

(49) Manenti, L.; Paganoni, P.; Floriani, I.; Landoni, F.; Torri, V.; Buda, A.; Taraboletti, G.; Labianca, R.; Belotti, D.; Giavazzi, R. *Eur. J. Cancer* **2003**, *39*, 1948–1956.

(50) Belotti, D.; Calcagno, C.; Garofalo, A.; Caronia, D.; Riccardi, E.; Giavazzi, R.; Taraboletti, G. *Mol. Cancer Res.* **2008**, *6*, 525–534.

FIGURE CAPTIONS

Figure 1. (a) Immobilization of Avastin on SPAnH-Fe_3O_4 nanoparticles. (b) TEM image of the SPAnH-Fe_3O_4. (c) TEM image of the Avastin-SPAnH-Fe_3O_4. (d) FT-IR spectra of the SPAnH-Fe_3O_4 nanoparticles, Avastin, and Avastin-SPAnH-Fe_3O_4. (e) Nyquist plot of bare Au (■), SPAnH-Fe_3O_4-modified Au (●) and Avastin-SPAnH-Fe_3O_4-modified Au (▲) electrodes. (f) Optimization of Avastin immobilization (n = 3).

Figure 2. (a) Photograph of a poly-SiNW-FET wafer. (b) Schematic diagram of a poly-SiNW-FET device. (c) FE-SEM image of a poly-SiNW-FET with a wire length × width of 2 μm × 0.3 μm. (d) I_{SD}-V_G curves of poly-SiNW-FET devices with a wire length × width (μm × μm) of 2 × 0.3 (■), 4 × 0.5 (▼), 4 × 0.3 (●), 13 × 0.5 (◆), and 13 × 0.3 (▲).

Figure 3. (a) Sketch of the surface modification of the poly-SiNW-FET devices. (b) Sketch of the Avastin-SPAnH-Fe_3O_4/poly-SiNW-FET biosensor preparation. (c) Current changes in the Avastin-SPAnH-Fe_3O_4/poly-SiNW-FET device for various wire length × width (μm × μm) combinations after hybridizing with 125 pg/mL VEGF (n = 3).

Figure 4. (a) I_{SD}-V_G curves of Avastin-SPAnH-Fe_3O_4/poly-SiNW-FET biosensors in the absence and presence of interfering species. (b) Effects of interfering species on the current variations in Avastin-SPAnH-Fe_3O_4/poly-SiNW-FET biosensors before (red bar) and after washing (green bar) (n = 3). (c) I_{SD}-V_G curves of Avastin-SPAnH-Fe_3O_4/poly-SiNW-FET biosensors with various VEGF concentrations. (d) Calibration curves of current responses to VEGF concentrations based on Avastin-SPAnH-Fe_3O_4/poly-SiNW-FET biosensors with (▒) and without (○) interfering species (n = 5).

Figure 5. Variations in the Avastin-SPAnH-Fe_3O_4/poly-SiNW-FET biosensors in response to VEGF (125 pg/mL) after storing at 4 °C (n = 3) for various days.

Figure 6. (a) VEGF concentrations in serum samples from patients suffering from the various stages of cervical cancer based on ELISA (red bar) and the Avastin-SPAnH-Fe_3O_4/poly-SiNW-FET (green bar) (n = 3). (b) VEGF concentrations in serum samples from healthy subjects based on the Avastin-SPAnH-Fe_3O_4/poly-SiNW-FET (n = 3). (c) Optical density (O.D.) calibration curve for VEGF concentrations based on ELISA (n = 3).

Figure 7. The VEGF (n = 5), CA-125, and CT (inset) measurements obtained pre-operation (yellow), post-operation in progress (green), and post-operation with Avastin therapy (white).

Figure 1

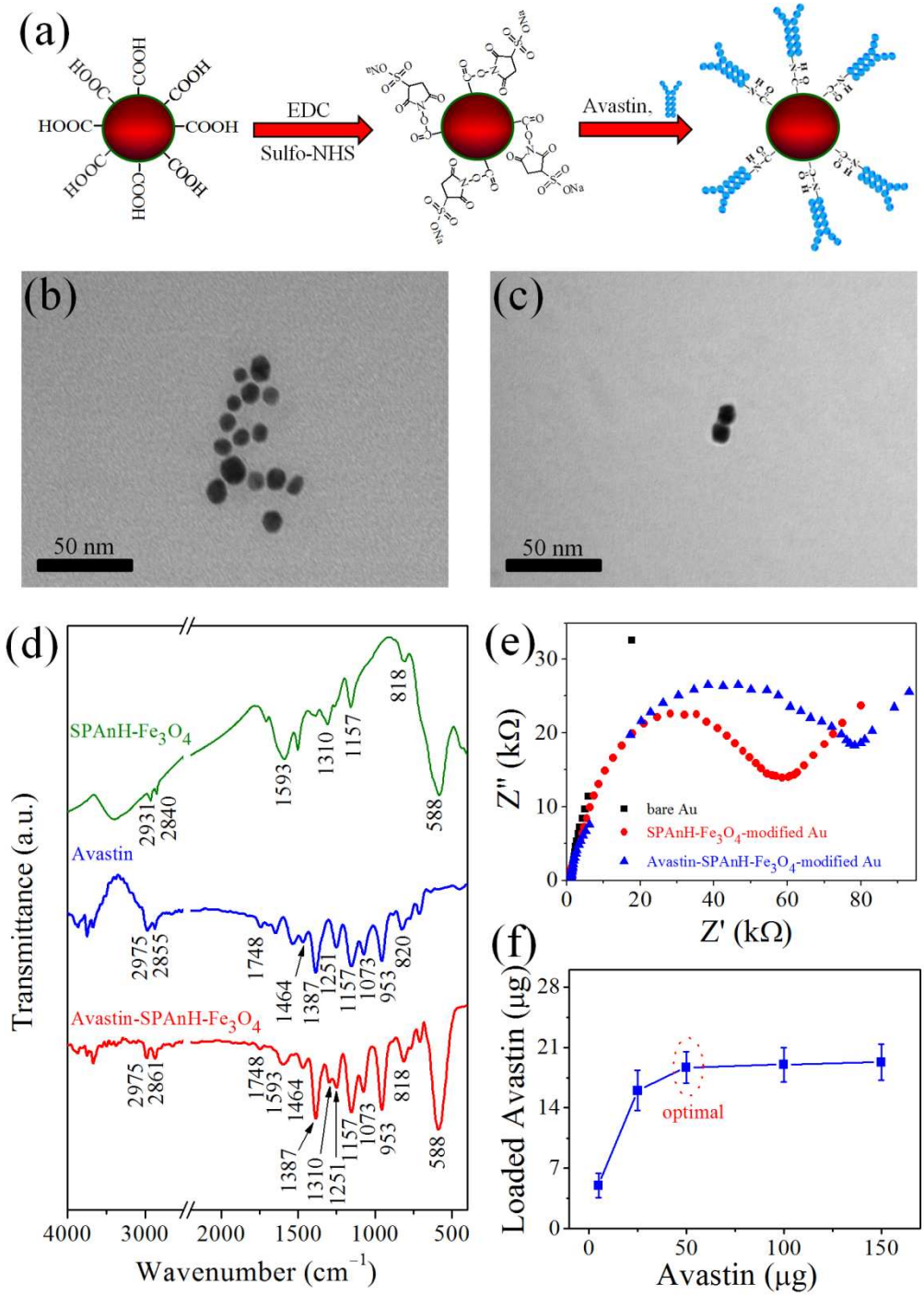
(a)
HOOC
COOH
EDC
Sulfo-NHS
Avastin
(b)
50 nm
(c)
50 nm
(d)
SPAnH-Fe3O4
Avastin
Avastin-SPAnH-Fe3O4
Transmittance (a.u.)
Wavenumber (cm−1)
(e)
Z'' (kΩ)
Z' (kΩ)
bare Au
SPAnH-Fe3O4-modified Au
Avastin-SPAnH-Fe3O4-modified Au
(f)
Loaded Avastin (μg)
Avastin (μg)
optimal

Figure 2

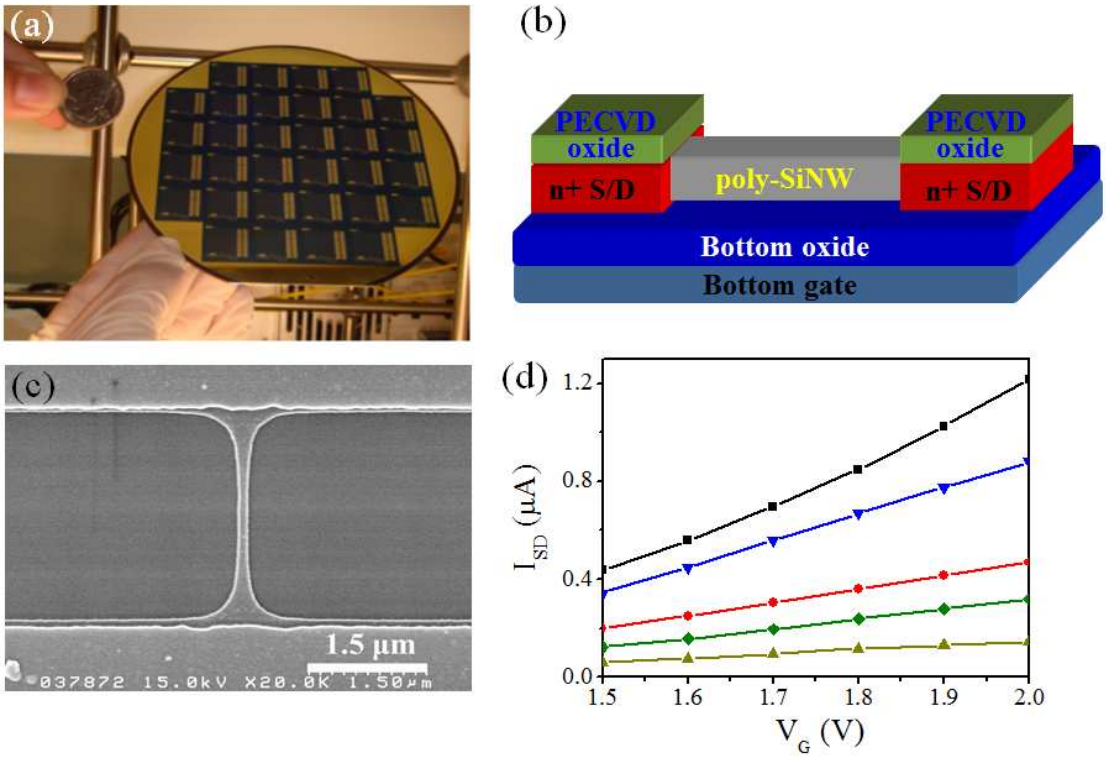
(a)
(b)
PECVD oxide
PECVD oxide
n+ S/D
poly-SiNW
n+ S/D
Bottom oxide
Bottom gate
(c)
1.5 µm
037872 15.0kV X20.0K 1.50µm
(d)
1.2
0.8
0.4
0.0
I_{SD} (µA)
1.5
1.6
1.7
1.8
1.9
2.0
V_G (V)

Figure 3

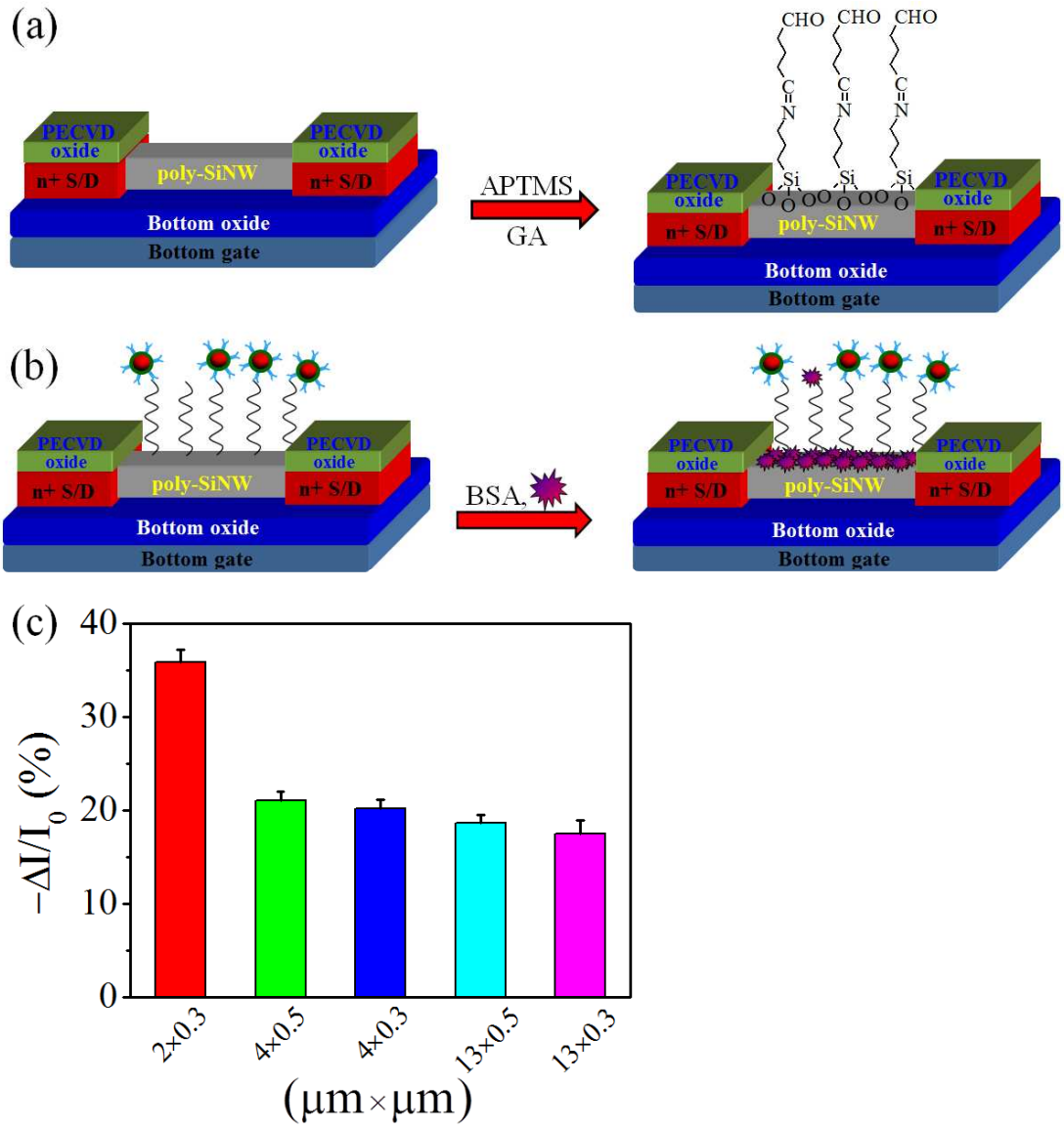
(a)
PECVD
oxide
n+ S/D
poly-SiNW
PECVD
oxide
n+ S/D
Bottom oxide
Bottom gate
APTMS
GA
CHO
CHO
CHO
C
N
Si
O
(b)
BSA
(c)
$-\Delta I/I_0$ (%)
0
10
20
30
40
2×0.3
4×0.5
4×0.3
13×0.5
13×0.3
(μm×μm)

Figure 4

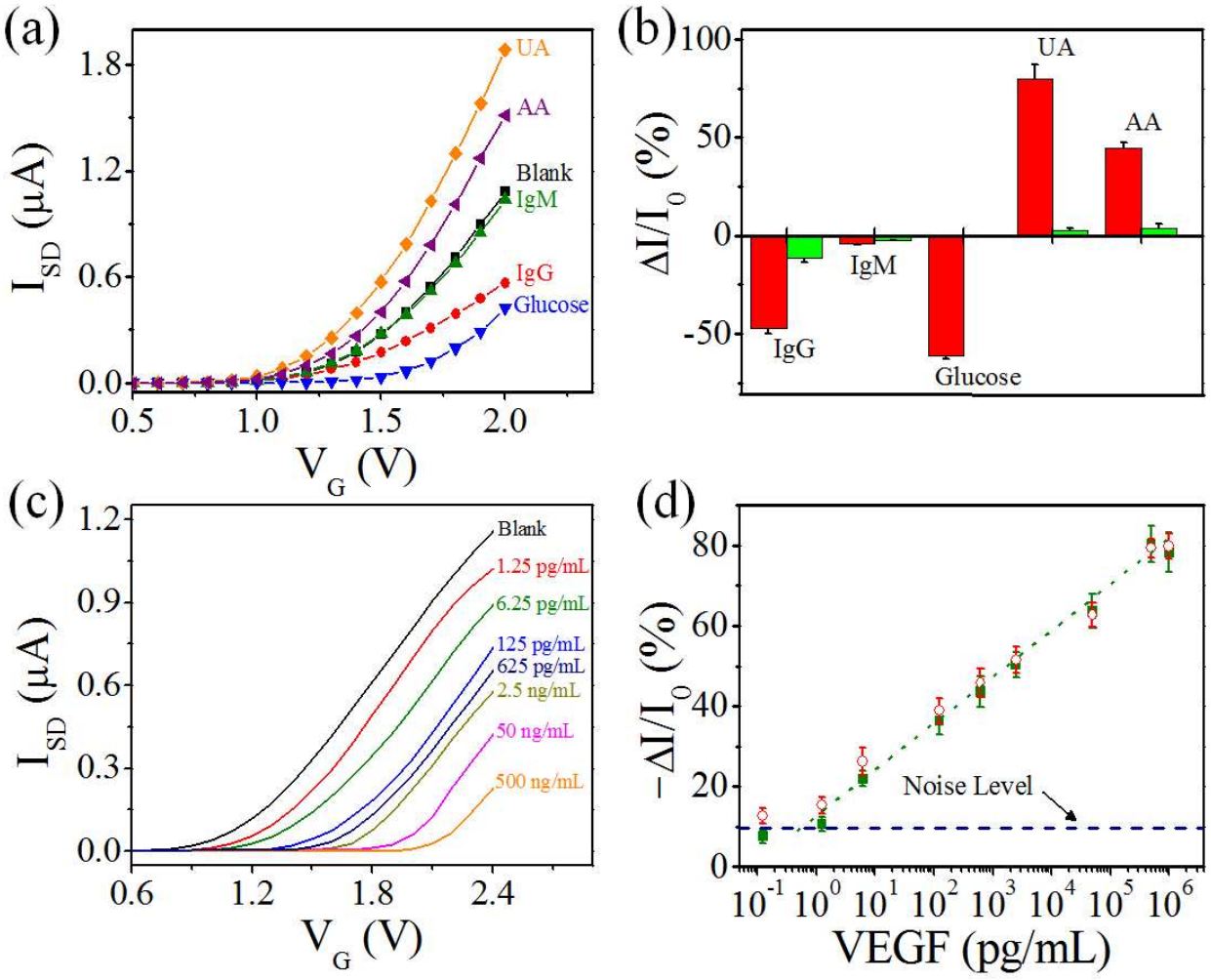
(a)
UA
AA
Blank
IgM
IgG
Glucose
I_{SD} (μA)
V_G (V)
(b)
UA
AA
IgM
IgG
Glucose
$\Delta I/I_0$ (%)
(c)
Blank
1.25 pg/mL
6.25 pg/mL
125 pg/mL
625 pg/mL
2.5 ng/mL
50 ng/mL
500 ng/mL
I_{SD} (μA)
V_G (V)
(d)
Noise Level
$-\Delta I/I_0$ (%)
VEGF (pg/mL)

Figure 5

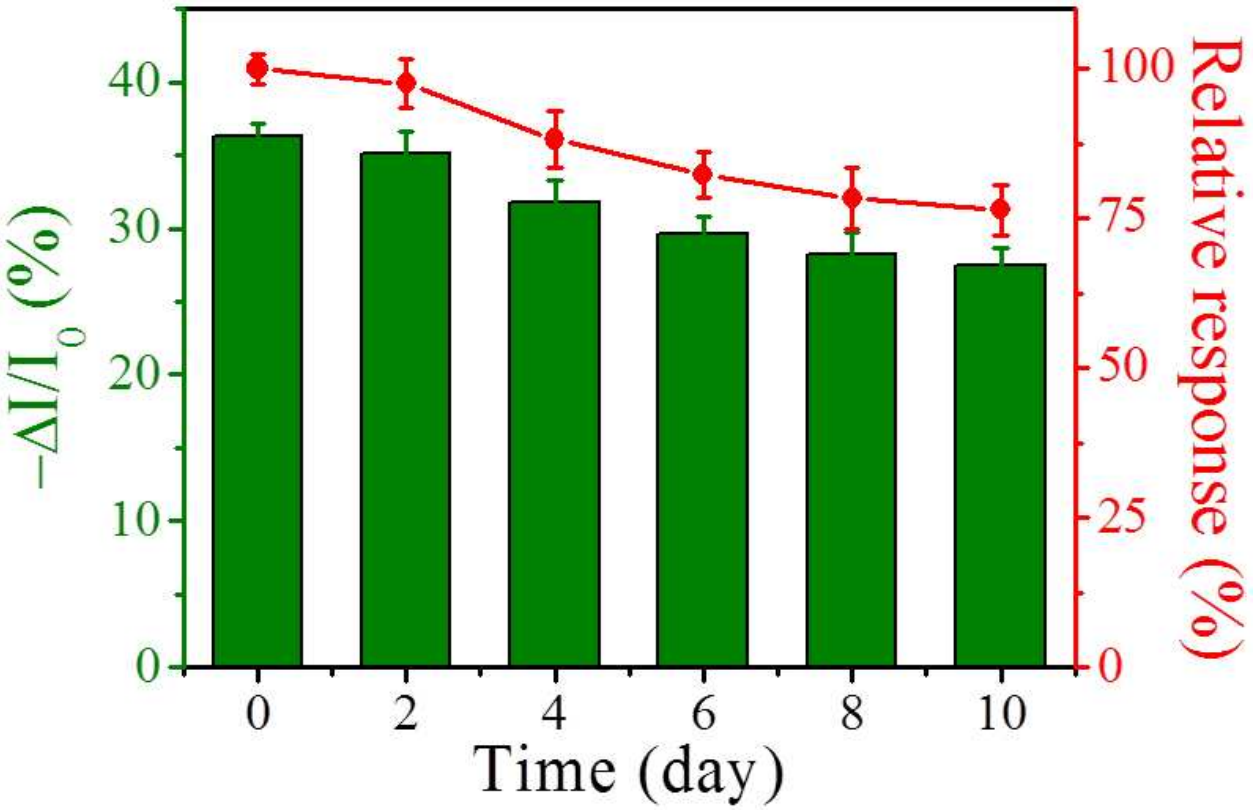
$-\Delta I/I_0$ (%)
Relative response (%)
Time (day)
0
10
20
30
40
0
25
50
75
100
0
2
4
6
8
10

Figure 6

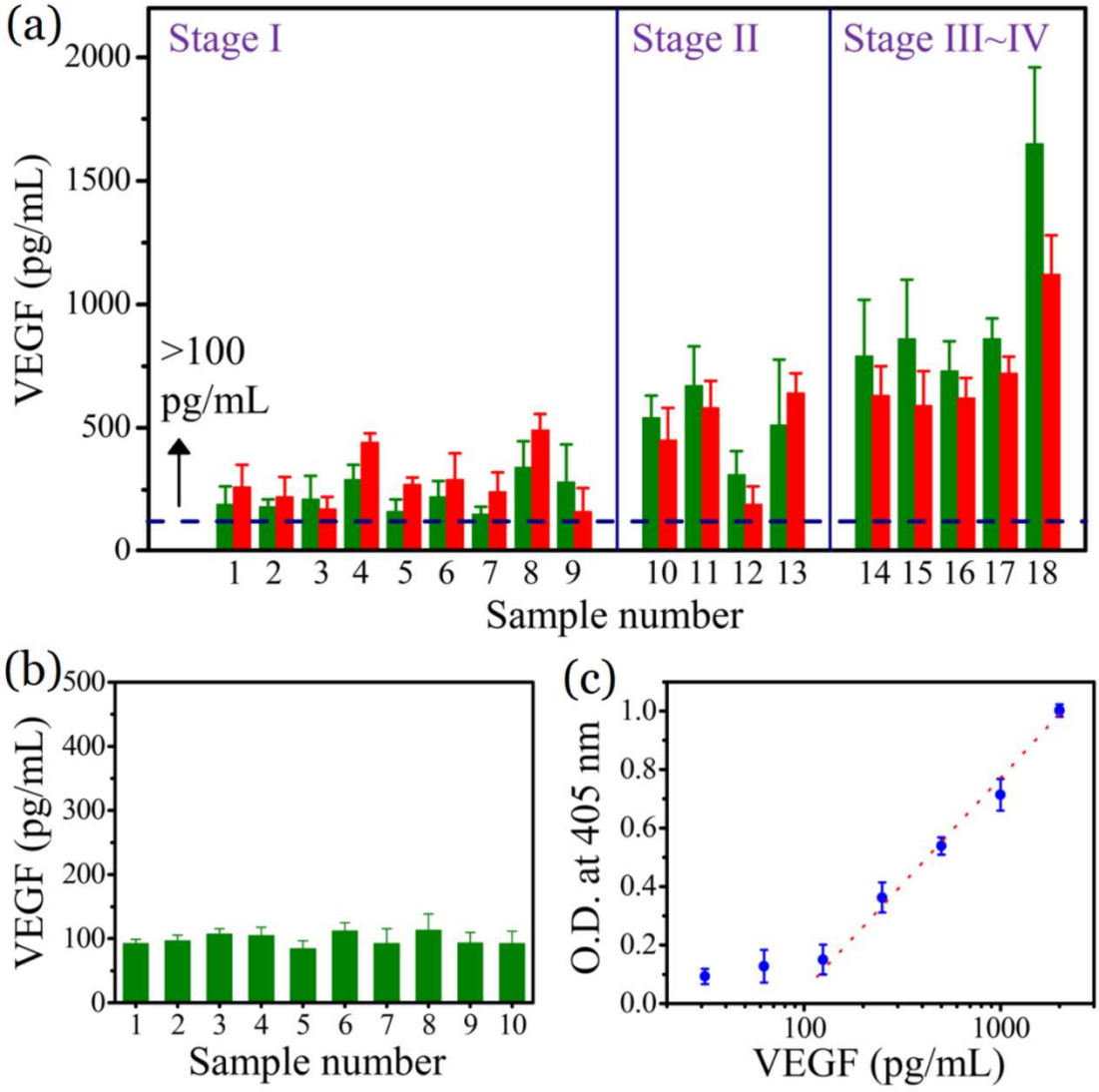
(a)
Stage I
Stage II
Stage III~IV
VEGF (pg/mL)
>100
pg/mL
Sample number
(b)
VEGF (pg/mL)
Sample number
(c)
O.D. at 405 nm
VEGF (pg/mL)

Figure 7

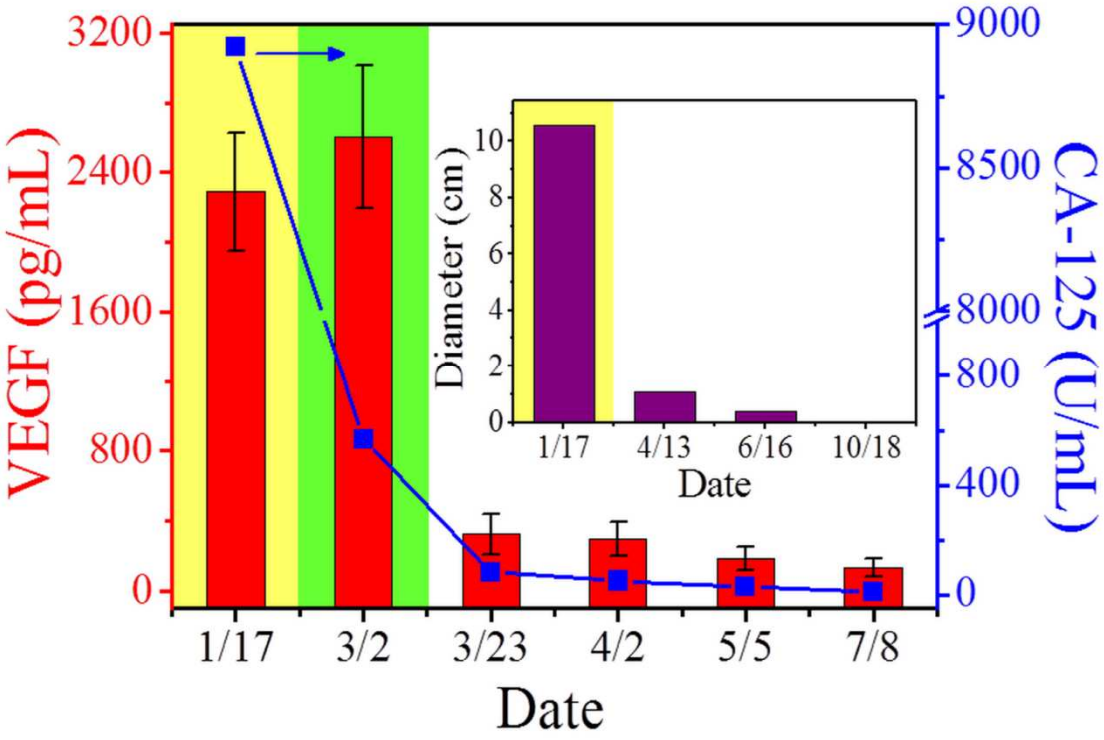
VEGF (pg/mL)
CA-125 (U/mL)
3200
2400
1600
800
0
9000
8500
8000
800
400
0
1/17
3/2
3/23
4/2
5/5
7/8
Date
Diameter (cm)
10
8
6
4
2
0
1/17
4/13
6/16
10/18
Date

For TOC only

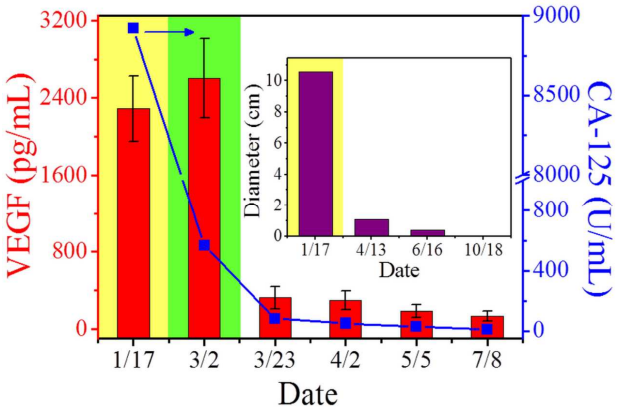

The VEGF (n = 5), CA-125, and CT (inset) measurements obtained pre-operation (yellow), post-operation in progress (green), and post-operation with Avastin therapy (white).